

Pseudo Rotary Resonance Relaxation Dispersion Effects in Isotropic Samples

Authors: Evgeny Nimerovsky*, Jonas Mehrens & Loren B. Andreas*

Affiliations:

Department of NMR based Structural Biology, Max Planck Institute for Multidisciplinary
Sciences, Am Faßberg 11, Göttingen, Germany

*Corresponding authors: land@mpinat.mpg.de ORCID: 0000-0003-3216-9065 and
evni@mpinat.mpg.de ORCID: 0000-0003-3002-0718.

Abstract

Enhanced transverse relaxation near rotary-resonance conditions is a well-documented effect for anisotropic solid samples undergoing magic-angle spinning (MAS). We report transverse signal decay associated with rotary-resonance conditions for rotating liquids, a surprising observation, since first-order anisotropic interactions are averaged at a much faster timescale as compared with the spinning frequency. We report measurements of ^{13}C and ^1H signal intensities under spin-lock for spinning samples of polybutadiene rubber, polyethylene glycol solution and 99.96% D_2O . A drastic reduction in spin-lock signal intensities is observed when the spin-lock frequency matches one or two times the MAS rate. In addition, oscillations of the signal are observed, consistent with a coherent origin of the effect, a pseudo rotary-resonance relaxation-dispersion (pseudo-RRD). Through simulations, we qualitatively describe the appearance of pseudo-RRD, which can be explained by time dependence caused by sample rotation and an

inhomogeneous field, the origin of which is an instrumental imperfection. Consideration of this effect is important for MAS experiments based on rotary-resonance conditions, and motivates the design of new MAS coils with improved rf-field homogeneity.

KEYWORDS: Magic-angle spinning, nuclear magnetic resonance spectroscopy, pseudo rotary-resonance relaxation-dispersion effect

Introduction

Measurement of the transverse relaxation rates of nuclear spins as a function of the applied rf-field spin-lock strengths is an elegant and well-established method for detecting structural molecular dynamics.(Abyzov et al., 2022; Alam et al., 2024; Camacho-Zarco et al., 2022; Hu et al., 2021; Massi and Peng, 2018; Palmer, 2015; Palmer and Massi, 2006; Pratihari et al., 2016; Rangadurai et al., 2019; Sekhar and Kay, 2019; Stief et al., 2024) For molecular solids, rocking motion or slow exchange in organic and inorganic samples(Fonseca et al., 2022; Keeler and McDermott, 2022; Krushelnitsky et al., 2018, 2023; Kurauskas et al., 2017; Lewandowski et al., 2011; Ma et al., 2014; Marion et al., 2019; Öster et al., 2019; Quinn and McDermott, 2009; Rovó and Linser, 2018; Shcherbakov et al., 2023; Vugmeyster et al., 2023) under MAS(Andrew et al., 1958; Lowe, 1959) NMR have been studied via the impact on transverse relaxation. This detection can be achieved by performing a spin-lock experiment,(Furman et al., 1998) where the decay of magnetization is measured as a function of the power of the applied spin-lock (SL) pulse. For slow motion or slow exchange in the microsecond (μ s) range, the spectral densities(Redfield, 1957) of the investigated spins may include additional terms(Kurbanov et al., 2011; Marion et al., 2019) that arise from non-averaged anisotropic interactions.(Kurbanov et al., 2011; Rovó, 2020; Schanda and Ernst, 2016) These terms depend on the sums and differences between the nutation frequency induced by the rf-field ($\nu_{SL}=\gamma B_1/(2\pi)$) and MAS rate (ν_R). Such

dependence causes a significant increase in the measured relaxation rates when ν_{SL} approaches one of the rotary-resonance conditions ($\nu_{SL} = \nu_R$ or $2\nu_R$). (Marion et al., 2019)

For liquid samples, where SL experiments are routinely used to detect fast exchange, (Cavanagh et al., 2006; Deverell et al., 1970; Palmer, 2004) sample rotation is not expected to induce any rotary-resonance conditions based on anisotropic spin interactions, (Levitt et al., 1988; Oas et al., 1988) since such interactions are eliminated by nanosecond-timescale isotropic motion. (Haeberlen and Waugh, 1968; Maricq, 1982) However, to our surprise, we still observed changes in the SL signals at rotary-resonance conditions for liquid and liquid-like samples during SL experiments. Since the signal decreases, but is also clearly oscillatory, a signature of coherent effects, we refer to this phenomenon as a pseudo rotary-resonance relaxation-dispersion (pseudo-RRD). A review of the literature revealed articles suggesting related resonance conditions for rotating liquid samples: in adiabatic TOCSY experiments, enhanced performance was observed under specific matching conditions in relation to the spinning frequency. (Kupče et al., 2001; Zektzer et al., 2005)

In this article, we measured pseudo-RRD for several liquid and liquid-like samples, and observe similar effects in each. Through numerical simulations, (Nimerovsky and Goldbourt, 2012) we show that this behavior can be qualitatively explained by the influence of the periodic component of the applied rf-field, which arises from the rotation of the sample in a spatially inhomogeneous rf-field. (Aebischer et al., 2021; Tošner et al., 2017)

Results and Discussion

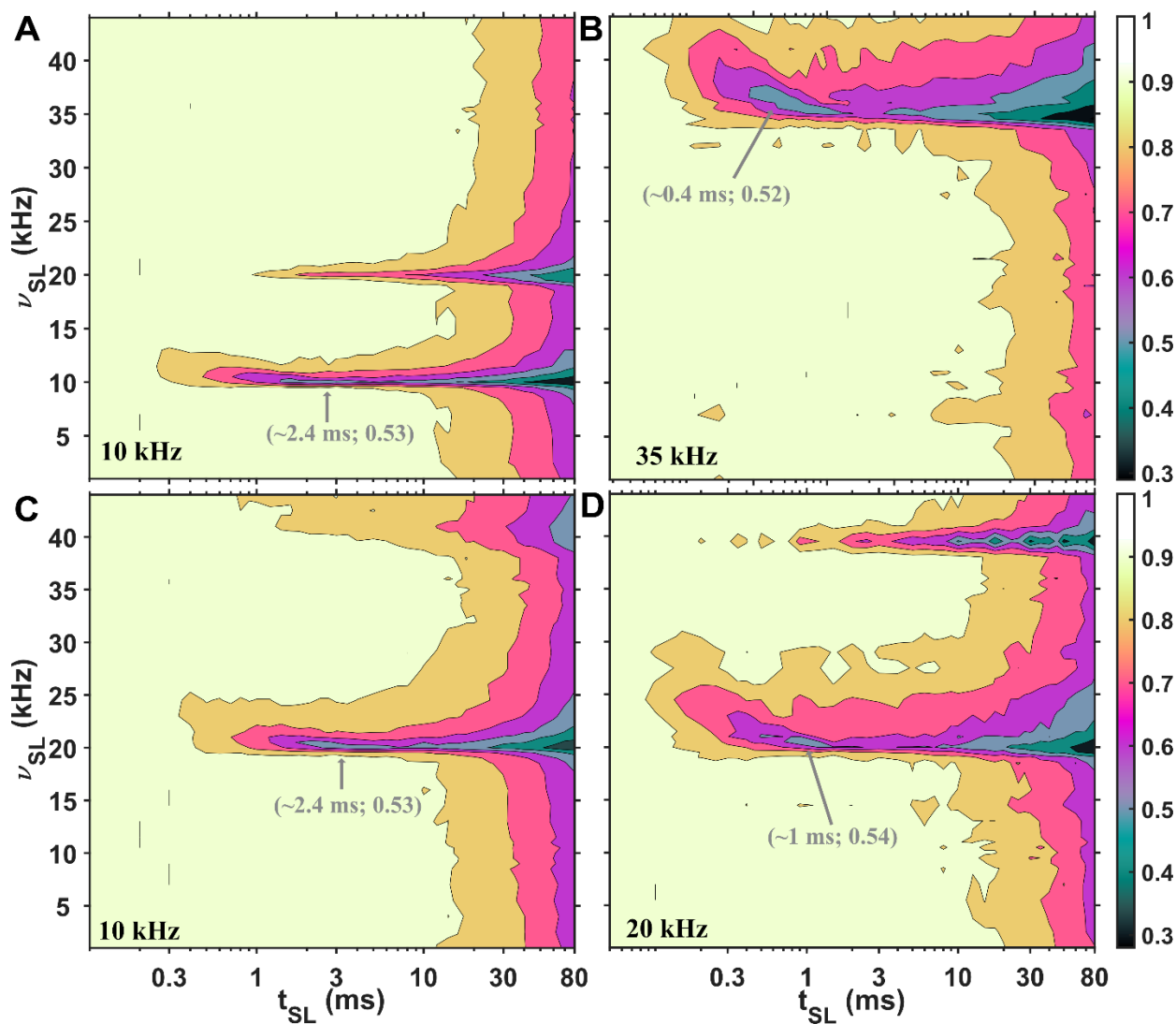
We measured pseudo RRD for natural abundance ^{13}C polybutadiene rubber at 10 kHz, 20 kHz and 35 kHz MAS. The same pseudo RRD behavior is observed for a polyethylene glycol

Figure 1 Spin-lock sequence with heat compensation (HC), T_2 –filter (2 ms – π -pulse – 2ms) and spin-lock (SL) blocks. The SL and HC elements consisted of a train of N_{SL} rotor-synchronized continuous (A) or windowed (B) pulses with the same phase (ϕ_2) and rf-field strength (ν_{SL}). In all experiments, $power_{HC} + power_{SL} = \text{constant}$ (equivalent to 50 kHz rf-field strength). During acquisition, WALTZ-16 decoupling(Shaka et al., 1983) (C) was applied on the ^1H channel.

The experimental ^{13}C polybutadiene rubber SL profiles (acquired with a 1.3 mm probe) under three different MAS rates: 10 kHz (A and C), 20 kHz (D) and 35 kHz (B) are shown in Figure 2. For Figures 2A, 2B and 2D, a drastic reduction in the SL signal is observed at rotary-resonance conditions when ν_{SL} equals either ν_R or $2\nu_R$. Together with reduction in the SL signal, oscillations are observed. For Figure 2C, we used 10 kHz MAS and windowed pulses: half of the rotor period is a window, as shown in Figure 1B. Again, a drastic reduction in the SL signal is observed, but when ν_{SL} equals either to $2\nu_R$ or $4\nu_R$. We previously observed similar behavior for windowed CP profiles,(Nimerovsky et al., 2023) where increasing the window between rotor-synchronized pulses from zero to half a rotor period doubled the required rf-field strength for cross-polarization transfers.(Hartmann and Hahn, 1962) Interestingly, with windowed pulses, the SL profile appears similar to that with continuous pulses, and even under a low rf-field strength of 1 kHz, there is no change in the SL signal intensities (Figure S1A in supplementary information, SI). The experimental spin-echo(Hahn, 1950) and inversion recovery(Vold et al., 1968) curves for this sample are illustrated in Figure S1A-B in [the SI](#).

From Figure 2, we can also observe that the location of the first minimum signal intensity in the experimental SL profiles depends on the MAS rate (indicated in gray in Figure 2). For 10 kHz MAS (Figure 2A and 2C), the locations are approximately at a 3 ms SL time, while for 20 kHz (Figure 2D) and 35 kHz (Figure 2B), the locations are approximately at 1 ms and 0.4 ms,

1 respectively. However, in all four profiles at these minimum points, the signal reaches a similar
 2 value of approximately 0.53.



3
 4 **Figure 2** ^{13}C polybutadiene rubber signal (the peak intensities) is shown as functions of the rf-field strength (ν_{SL} , y-
 5 axis) and mixing time (t_{SL} , x-axis) of the SL under three different MAS rates: 10 kHz (A and C), 20 kHz (D) and 35
 6 kHz (B). For (A), (B) and (D), continuous SL was applied, while for (C), windowed (half rotor period was filled
 7 with the pulse) SL was implemented. The values in gray represent the coordinates of the first minimum in the
 8 profiles. Additional experimental details are provided in the SI.

Rotary-resonance conditions at ν_R and $2\nu_R$ of rf-field strength are also observed for the polyethylene glycol (Figure 3B, acquired with a 4 mm probe) and for residual protons in liquid deuterium oxide samples (Figure 3D, acquired with a 1.3 mm probe). The 1D spectra of these samples are shown in Figure 3A and C, for PEG and liquid water. For each sample, two rotary-resonance conditions are observed at positions equal to integer multiplies of the MAS rates ($\nu_{SL} = \nu_R, 2\nu_R$). For liquid water (Figure 3D), the additional rotary-resonance condition with $n=3$ appears very weakly. We more carefully sampled around this condition for the water sample.

The performance of the SL experiments on all three samples helps rule out the influence of translational diffusion(Hahn, 1950) (which may be present for polyethylene glycol and liquid water but not for polybutadiene rubber) or residual dipolar interaction(Cohen-Addad and Vogin, 1974) (which might be present for polybutadiene rubber but is not relevant for polyethylene glycol and liquid water).

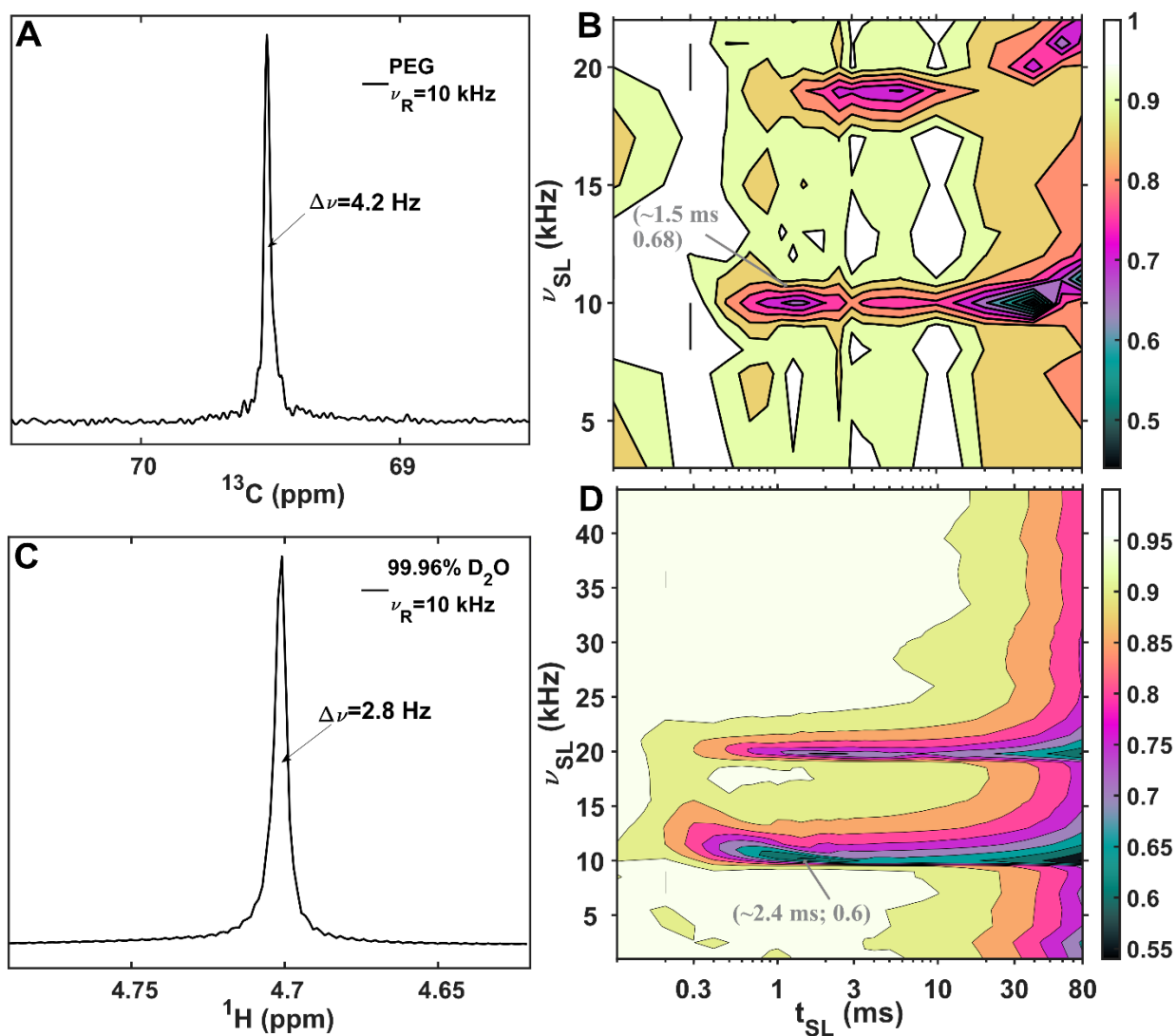


Figure 3 ^{13}C and ^1H spin-lock profiles at 10 kHz MAS. (A-B) Single-pulse ^{13}C spectra and SL profile of polyethylene glycol (PEG) acquired with a 4 mm probe. (C,D) ^1H single pulse and SL profile of 99.96% D_2O acquired with a 1.3 mm probe. The profiles in (B,D) show ^{13}C and ^1H signal amplitudes (peak intensities) as a function of the rf-field strength (ν_{SL} , y-axis) and mixing time (t_{SL} , x-axis) of the SL pulse. The values in gray are the coordinates of the first minimum in the profiles. Additional experimental details are provided in the SI.

To identify the major source of the apparent rotary-resonance conditions in liquid and liquid-like samples, we performed theoretical and numerical analysis of the spin-lock (SL) signal (Eqns. 1-7 below). In this analysis, three possible sources of pseudo-RRD are considered, all of which are time-dependent periodic functions. The first two are related to B_0 and B_1 modulations,

1 which arise from the rotation of the sample within inhomogeneous B_0 or B_1 fields. Note that the
2 B_0 field refers to the main field, and that modulations in B_0 can be in any direction. Similarly, B_1
3 field modulations can occur in any direction, and z-direction modulations are particularly
4 relevant for a solenoid at the magic angle. The precise distribution of B_0 or B_1 fields in MAS
5 probes have been previously investigated.(Engelke, 2002; Gupta et al., 2015; Hoult, 1976;
6 Hürlimann and Griffin, 2000; Paulson et al., 2004; Tošner et al., 2017, 2018) Here we consider a
7 simplified model of field distributions in order to reveal the dependence on MAS rates, rather
8 than predict the exact behavior of a particular probe. Note that the consideration of spatially
9 distributed B_0 field inhomogeneity is compatible with a narrow linewidth under MAS.(Sodickson
10 and Cory, 1997) For completeness of the theoretical analysis, a dipolar interaction between a pair
11 of spins was also included as a third possible source, although it may be disregarded since the
12 rotary-resonance effect was observed for ^1H spins in 99.96% D_2O (Figure 3A-B).

13 The effects of inhomogeneous rf-field on MAS spectra have been investigated
14 previously.(Aebischer et al., 2021; Goldman and Tekely, 2001; Tekely and Goldman, 2001;
15 Tošner et al., 2017) Rather than B_1 oscillations, the coil receptivity was shown to oscillate due to
16 rotation of the sample relative to the coil, and the authors showed that this instrumental
17 imperfection results in the appearance of sidebands that are unrelated to the chemical shift
18 anisotropy (CSA).(Goldman and Tekely, 2001; Tekely and Goldman, 2001) Sidebands due to
19 rotation through inhomogeneous B_0 and B_1 fields is a well-known effect in liquids.(Malinowski
20 and Pierpaoli, 1969; Vera and Grutzner, 1986) For solid samples, Aebischer et al.(Aebischer et
21 al., 2021) investigated the influence of time-dependent modulations of the rf-field amplitude and
22 phase on the performance of selected recoupling sequences and nutation experiments. In this
23 case, the modulations did not significantly affect most recoupling sequences, with the exception

of double quantum C-symmetry sequences.(Lee et al., 1995) It was noted much earlier that oscillations in phase were needed to fully explain experimental results in rotary resonance recoupling.(Levitt et al., 1988) Consistent with the matching conditions identified in this study, Aebischer et al.(Aebischer et al., 2021) revealed significant effects at ν_R and $2\nu_R$ in nutation spectra. The distribution of B_1 fields in a solenoidal coil was elegantly visualized in SL experiments of solid samples, in which case the loss of signal at rotary resonance was interpreted as CSA recoupling.(Tošner et al., 2017)

To understand the origin of the pseudo-RRD effect, we start with the simplest case, investigating the behavior of an on-resonance spin (I) during the rf-field spin-lock. The simulated SL-signal is defined as follows:

$$S_{SL}(t_{SL}) = \text{Tr} \left\{ I_x \hat{T} e^{-i \int_0^{t_{SL}} dt H'_{\text{total}}} I_x \hat{T} e^{i \int_0^{t_{SL}} dt H'_{\text{total}}} \right\}, \quad \text{Eqn. (1)}$$

where \hat{T} is a Dyson operator and H'_{total} is a total Hamiltonian. We consider the effects of B_0 and B_1 modulations or dipolar interaction. For all three sources, H'_{total} can be defined as follows:

$$H'_{\text{total}} = H'_{SL} + H'_t = \omega_{SL} I_x + 2\pi \sum_n a_n \cos(n\omega_R t + \phi_n) [I_z \cos\varphi + I_y \sin\varphi] \widehat{O_p}, \quad \text{Eqn. (2)}$$

where $\omega_{SL} = 2\pi\nu_{SL}$ and H'_{SL} is an ideal spin-lock Hamiltonian. Here, $\widehat{O_p} = 1$ for a single spin with B_0 ($\varphi \geq 0$) or B_1 ($\varphi = \pi/2$) modulations, or $\widehat{O_p} = 2S_z$ with $\varphi = 0$ for a two-spin system (dipolar interaction). While for dipolar interaction, n is 1 or 2,(Mehring, 1983; Olejniczak et al., 1984) for B_0 and B_1 modulations, n may take any integer value.(Aebischer et al., 2021) This is because these modulations are not purely sinusoidal; there are contributions from overtone frequencies. In the experimental SL profiles (Figures 2 and 3), two rotary-resonance conditions are clearly observed. Therefore, in the following discussion, $n = 1, 2$ will be considered for all

three cases. Note also that for the cosine modulated terms of Eqn. 2, only I_y (and not I_z) survives the rotating frame transformation and secular approximation for the case of B_1 modulation. Both terms are relevant for B_0 modulations. For the dipolar interaction, a_k inversely depend on the distance between the pair of spins and the orientation: (Mehring, 1983; Olejniczak et al., 1984) $a_1 = \frac{v_D}{\sqrt{2}} \sin(2\beta)$ and $a_2 = -\frac{v_D}{2} \sin^2(\beta)$; $v_D = v_{D,IS} = -\frac{\mu_0}{8\pi^2} \frac{\hbar \gamma_I \gamma_S}{r_{IS}^3}$ and (β) is the Euler angle with respect to the rotor frame. (Mehring, 1983) For B_0 and B_1 modulations, a_k values do not exhibit any orientation dependence. It is worth noting that for B_1 modulations, a_k values change with the strength of the applied rf-field lock value (v_{SL}). If φ does not vary with time, Eqn. (2) can be simplified by rotation of H'_{total} by an φ angle around the \hat{x} using the operator $e^{i\varphi I_x}$. Such a rotation removes any dependence on φ , since the initial and the final operators in Eqn. (1) commute with $e^{i\varphi I_x}$. The modified Eqn. (2) is written as follows:

$$H_{total} = e^{-i\varphi I_x} H'_{total} e^{i\varphi I_x} = H_{SL} + H_t = \quad \text{Eqn. (3)}$$

$$\omega_{SL} I_x + 2\pi \sum_n a_n \cos(n\omega_R t + \phi_n) I_z \widehat{O} p_z$$

Thus, while B_0 modulation may occur anywhere in the yz -plane, the theoretical treatment remains exactly the same as for z modulation. Mathematically, this is also true for B_1 modulation, while physically, these modulations are only relevant when in the transverse plane. In the SI, using average Hamiltonian theory (AHT) and considering only the first-order terms (Haeberlen and Waugh, 1968) under rotary-resonance conditions ($v_{SL} = \nu_R$ or $2\nu_R$), the measured SL-signal for B_0 or B_1 modulations is as follows:

$$S_{SL}(t_{SL} = N_{SL} T_R) \approx \cos(\pi a_k t_{SL}), \quad \text{Eqn. (4)}$$

while for dipolar interaction:

$$S_{SL}(t_{SL} = N_{SL}T_R) \approx \int d\Omega \cos(\pi a_k t_{SL}). \quad \text{Eqn. (5)}$$

where the integration over orientation (Ω) indicates the powder averaging with Euler angles, (α, β, γ). (Mehring, 1983) The derivations of Eqn.(5) and Eqn.(6) are shown in the SI (Eqns. (S1)-(S11)).

The complete agreement between AHT and numerical simulations of SL-signals (Figures S3-S4 in the SI) indicates that this effect is fully coherent in origin. The change in MAS rate affects only B_1 -induced signal modulations (Figures S4 and S5), since the B_1 field is also increased at the resonance condition. Specifically, the strength of field oscillations (a_k) increases linearly with the B_1 field, which matches the MAS frequency at the resonance condition, and therefore the signal modulation frequency also increases linearly. In the case of B_0 modulation, adjustments to the shimming coil are expected to have a profound effect, but oscillations in signal amplitude are expected to be independent of the applied B_1 field. By contrast, for B_1 modulation, changes in the strength of the applied spin-lock have a major effect, since the oscillation frequency of signal amplitude is expected to depend on B_1 . These observations already point to B_1 as the most likely source of the observed pseudo-RRD effect, since the position of the first signal minimum was observed to profoundly depend on the MAS frequency (Figure 2).

A better match between experiment and simulation logically requires consideration of distributions in various parameters representing the position dependence of sample. Based on Figure S5, for all three sources, the rotary-resonance conditions are very narrow. However, the addition of the spatial distribution of the applied v_{SL} values to H_{SL} , broadens these conditions (Eqn. (S14) and Figure S6 in the SI), making them more experimentally detectable and damping oscillations.

1 More generally, it makes sense to also consider distributions in the amplitude of B_0 or B_1
 2 modulations (Eqns. (S15) and (S16) in the SI). The specific spatial distributions chosen for B_0
 3 and B_1 are summarized in Table S1 and shown in Figures S7 and S8 in the SI. The types of
 4 inhomogeneity used roughly match the expectation for solenoidal coils, where the sample near
 5 the ends of the coil experiences a lower rf-field strength. Figures 4-5 show simulations for B_0
 6 and B_1 modulation that include these distributions. The inclusion of distributions in the
 7 simulation primarily broadens the rotary-resonance conditions and affects the frequency and
 8 amplitude of the modulations in the spin-lock signals. Relatively good agreement is observed
 9 between the experiment and simulation despite the imprecise simulation of the spatial
 10 distributions of B_1 . A more quantitative assessment would call for calculation of the exact values
 11 and shapes of B_1 fields for a particular coil, as well as better characterization of B_0
 12 distributions.(Aebischer et al., 2021; Engelke, 2002; Guenneugues et al., 1999; Hürlimann and
 13 Griffin, 2000; Lips et al., 2001; Odedra and Wimperis, 2013; Paulson et al., 2004; Privalov et al.,
 14 1996; Schönzart et al., 2024; Tošner et al., 2017, 2018) Note that the distributions are reasonable,
 15 considering the published calculations for solenoidal coils.(Gupta et al., 2015; Tošner et al.,
 16 2017; Uribe et al., 2024)
 17 Figure 4 shows simulations for B_0 modulation that include distributions in SL frequency and in
 18 amplitude of B_0 modulation. While some similarities are seen as compared with the experimental
 19 data (Figure 2), there are three major differences in the SL profiles, which should be highlighted.
 20 Firstly, in Figure 4, the intensities at the first minima show a dependence on MAS rate (marked
 21 in gray in Figure 4), whereas in Figure 2, the experimental profiles show only a slight
 22 dependence. Secondly, in Figure 4, the locations of these minima in time (x-axis) do not depend
 23 on the MAS rate (Figure 4A, 4B and 4D), but are different when windowed pulses are applied

(Figure 4C). In contrast, the experimental profiles exhibit the reverse behavior. Thirdly, with windowed pulses, Figure 4C, the second rotary-resonance condition is attenuated compared to continuous spinlock, while in Figure 2C, two rotary-resonance conditions are clearly detected. Additionally, increasing the magnetic field inhomogeneity by deliberately mis-setting the room temperature shims had little influence on the SL profile (shown in Figure S2 in the SI). All of this indicates that a B₀ modulation cannot be a major source of the appearance of rotary-resonances conditions in these rotating liquids and liquid-like samples.

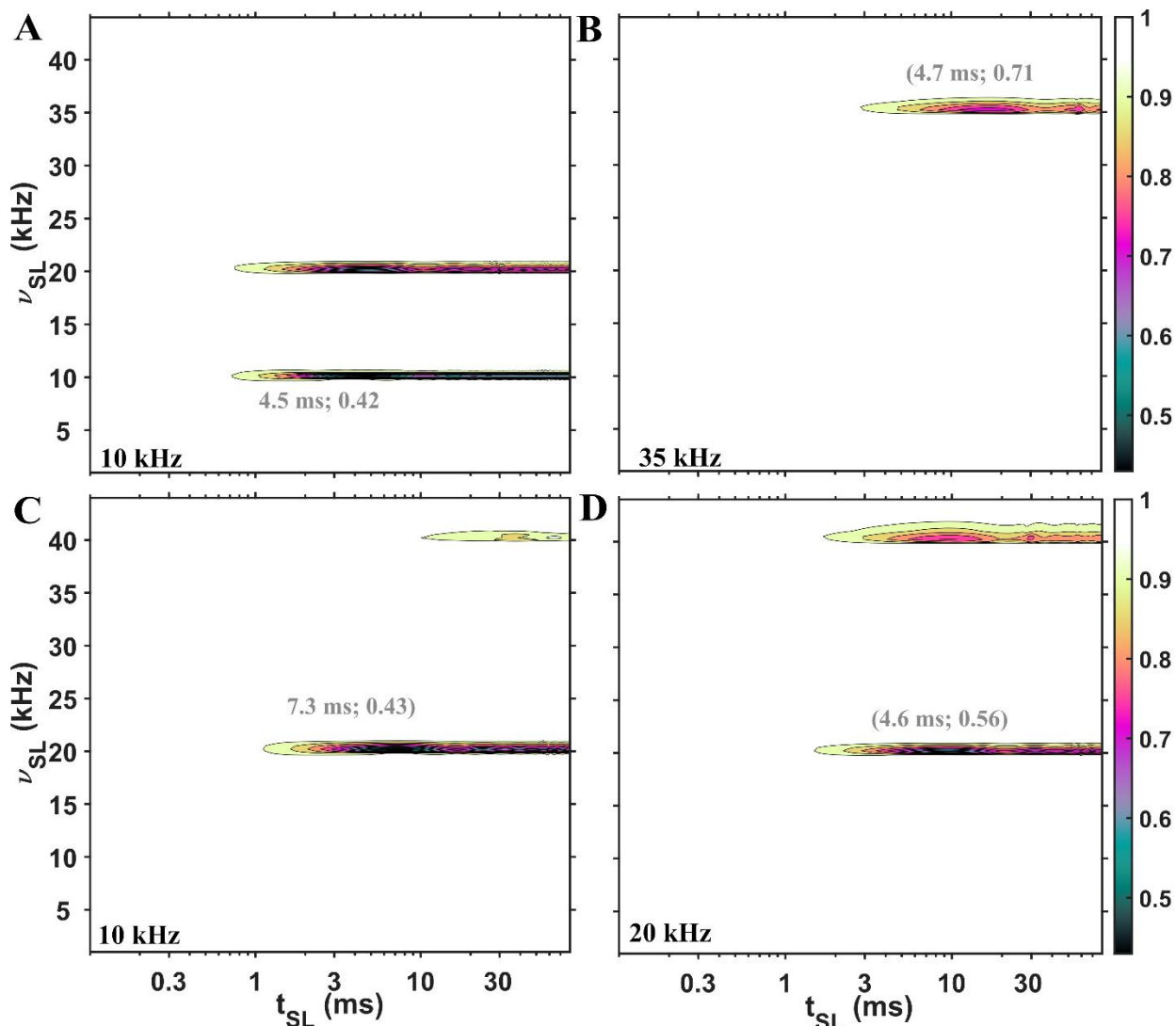


Figure 4 Simulated SL profiles showing the influence of time dependence introduced via B_0 modulation, including distributions in SL frequency and in amplitude of B_0 modulation. The simulated signal is shown as a function of the rf-field strength (ν_{SL} , axis y) and mixing time (t_{SL} , axis x) of the SL under three different MAS rates: 10 kHz (A and C), 20 kHz (D) and 35 kHz (B). For (A), (B) and (D), continuous SL was applied, while for (C) windowed SL was implemented (half rotor period was filled with the pulse). The values in gray represent the coordinates of the first minima in the profiles. No phenomenological relaxation was included in the simulations. Additional simulated details are provided in the SI.

In contrast, simulations of SL profiles with time dependence introduced via B_1 modulation (Figure 5) qualitatively agree with the experimental plots, indicating that a B_1 modulation is a better explanation for the appearance of rotary-resonance conditions in rotating liquids and liquid-like samples using conventional MAS NMR probes with solenoidal coils. Hardware limitations, including such time dependence has been previously considered in the design of magnetization transfer elements using optimal control. (Blahut et al., 2022, 2023; Glaser et al., 2015; Joseph and Griesinger, 2023; Tošner et al., 2017, 2018)

This qualitative explanation, provided by simulations, indicates that this effect can also be anticipated in experiments involving solid samples, in addition to the desired effects caused by molecular motion. It is therefore recommended to consider coil inhomogeneity when measuring relaxation rates near rotary resonance conditions. Fortunately, the magnitude of this effect is considerably smaller than the strong relaxation observed in recent reports that detected slow structural dynamics via near rotary resonance conditions. (Krushelnitsky et al., 2018)

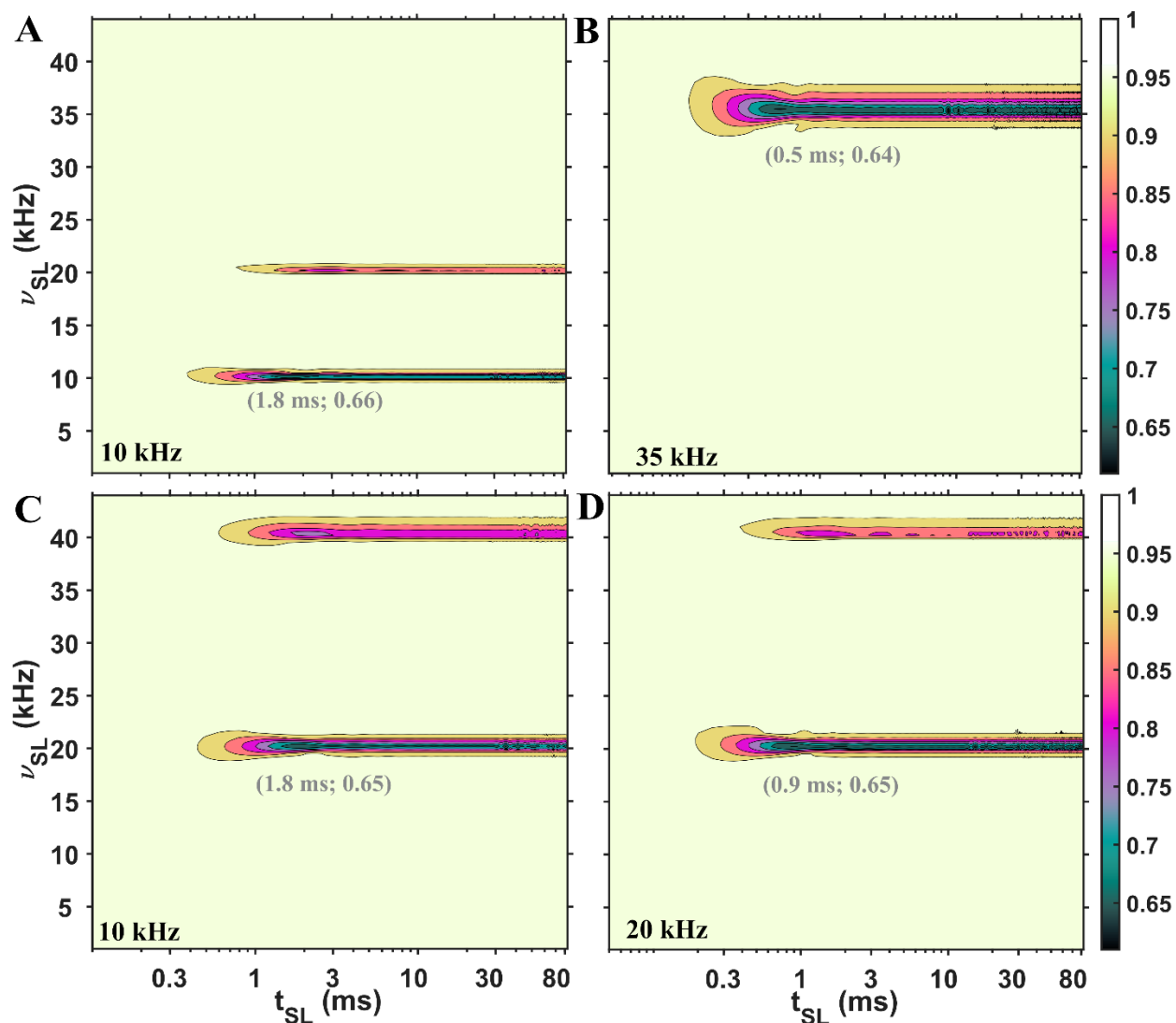


Figure 5 Simulated SL profiles showing the influence of time dependence introduced via B_1 modulation, including distributions in SL frequency and in amplitude of B_1 modulation. The simulated signal is shown as functions of the rf-field strength (ν_{SL} , axis y) and mixing time (t_{SL} , axis x) of the SL under three different MAS rates: 10 kHz (A and C), 20 kHz (D) and 35 kHz (B). For (A), (B) and (D), continuous SL was applied, while for (C) windowed (half rotor period was filled with the pulse) SL was implemented. The values in gray represent the coordinates of the first minima points in the profiles. Relaxation was not included in the simulations. Additional simulated details are provided in the SI.

Conclusions

Rotary-resonance conditions, under which the applied rf-field strength equals an even multiple of the MAS rate, provide a powerful avenue to obtain specific structural information via recoupling of anisotropic interactions in solids(De Paëpe, 2012; Nishiyama et al., 2022) or for detecting changes in the relaxation rates due to slow motion in the μs range.(Rovó, 2020)

Canonically, rotary-resonance conditions are not expected in liquids due to the averaging of first-order anisotropic interactions from (sub) nanosecond isotropic motion.(Haeberlen and Waugh, 1968; Maricq, 1982) In this article, we presented experimental data, in which we detected rotary-resonance conditions in a liquid and a liquid-like samples. We qualitatively explained the major source of these conditions, which can occur from a combination of two factors: the rotation of the sample and a spatially inhomogeneous rf-field produced a solenoidal coil.(Tošner et al., 2017) As a result, the rf-field Hamiltonian contains time-dependent terms, which leads to signal decrease, i.e. pseudo relaxation behavior, at or near rotary-resonance conditions. To mitigate these effects, it may be advantageous to consider different hardware designs,(Chen et al., 2018; Xu et al., 2021) for example rf coils that produce more homogeneous rf-fields.(Grant et al., 2010; Kelz et al., 2019; Krahn et al., 2008; Stringer et al., 2005)

Competing interests

The contact author has declared that none of the authors has any competing interests.

Acknowledgments

We acknowledge financial support from the MPI for Multidisciplinary Sciences, and from the Deutsche Forschungsgemeinschaft (Emmy Noether program Grant AN1316/1-2). We thank Dr. Supriya Pratihar for inspiring this work by noticing pseudo-RRD at rotary resonance conditions in exploratory high-power relaxation dispersion measurements in a 0.7 mm MAS probe. We thank Dr. Dirk Bockelmann and Brigitta Angerstein for technical assistance.

1 **Author contribution**

2 EN and LBA designed the experiments. EN and JM recorded NMR data and ran simulations, EN
3 and LBA wrote the article. All authors edited and approved the article.

4 **References**

- 5 Abyzov, A., Blackledge, M., and Zweckstetter, M.: Conformational Dynamics of Intrinsically Disordered
6 Proteins Regulate Biomolecular Condensate Chemistry, *Chem. Rev.*, 122, 6719–6748,
7 <https://doi.org/10.1021/acs.chemrev.1c00774>, 2022.
- 8 Aebischer, K., Tošner, Z., and Ernst, M.: Effects of radial radio-frequency field inhomogeneity on MAS
9 solid-state NMR experiments, *Magn. Reson.*, 2, 523–543, <https://doi.org/10.5194/mr-2-523-2021>, 2021.
- 10 Alam, M. K., Bhuvaneshwari, R. A., and Sengupta, I.: 19F NMR relaxation of buried tryptophan side
11 chains suggest anisotropic rotational diffusion of the protein RfaH, *J. Biomol. NMR*,
12 <https://doi.org/10.1007/s10858-024-00450-x>, 2024.
- 13 Andrew, E. R., Bradbury, A., and Eades, R. G.: Nuclear Magnetic Resonance Spectra from a Crystal
14 rotated at High Speed, *Nature*, 182, 1659–1659, <https://doi.org/10.1038/1821659a0>, 1958.
- 15 Blahut, J., Brandl, M. J., Pradhan, T., Reif, B., and Tošner, Z.: Sensitivity-Enhanced Multidimensional
16 Solid-State NMR Spectroscopy by Optimal-Control-Based Transverse Mixing Sequences, *J. Am. Chem.*
17 *Soc.*, <https://doi.org/10.1021/jacs.2c06568>, 2022.
- 18 Blahut, J., Brandl, M. J., Sarkar, R., Reif, B., and Tošner, Z.: Optimal control derived sensitivity-enhanced
19 CA-CO mixing sequences for MAS solid-state NMR – Applications in sequential protein backbone
20 assignments, *J. Magn. Reson. Open*, 16–17, 100122, <https://doi.org/10.1016/j.jmro.2023.100122>, 2023.
- 21 Camacho-Zarco, A. R., Schnapka, V., Guseva, S., Abyzov, A., Adamski, W., Milles, S., Jensen, M. R., Zidek,
22 L., Salvi, N., and Blackledge, M.: NMR Provides Unique Insight into the Functional Dynamics and
23 Interactions of Intrinsically Disordered Proteins, *Chem. Rev.*, 122, 9331–9356,
24 <https://doi.org/10.1021/acs.chemrev.1c01023>, 2022.
- 25 Cavanagh, J., Fairbrother, W. J., Palmer, A. G., III., Rance, M., and Skelton, N. J.: *Protein NMR*
26 *Spectroscopy: Principles and Practice*, 1 pp., 2006.
- 27 Chen, P., Albert, B. J., Gao, C., Alaniva, N., Price, L. E., Scott, F. J., Saliba, E. P., Sesti, E. L., Judge, P. T.,
28 Fisher, E. W., and Barnes, A. B.: Magic angle spinning spheres, *Sci. Adv.*, 4, eaau1540,
29 <https://doi.org/10.1126/sciadv.aau1540>, 2018.
- 30 Cohen-Addad, J. P. and Vogin, R.: Molecular Motion Anisotropy as Reflected by a “Pseudosolid” Nuclear
31 Spin Echo: Observation of Chain Constraints in Molten cis-1, 4-Polybutadiene, *Phys. Rev. Lett.*, 33, 940–
32 943, <https://doi.org/10.1103/PhysRevLett.33.940>, 1974.

1 De Paëpe, G.: Dipolar Recoupling in Magic Angle Spinning Solid-State Nuclear Magnetic Resonance,
2 Annu. Rev. Phys. Chem., 63, 661–684, <https://doi.org/10.1146/annurev-physchem-032511-143726>,
3 2012.

4 Deverell, C., Morgan, R. E., and Strange, J. H.: Studies of chemical exchange by nuclear magnetic
5 relaxation in the rotating frame, Mol. Phys., 18, 553–559, <https://doi.org/10.1080/00268977000100611>,
6 1970.

7 Engelke, F.: Electromagnetic wave compression and radio frequency homogeneity in NMR solenoidal
8 coils: Computational approach, Concepts Magn. Reson., 15, 129–155,
9 <https://doi.org/10.1002/cmr.10029>, 2002.

10 Fonseca, R., Vieira, R., Sardo, M., Marin-Montesinos, I., and Mafra, L.: Exploring Molecular Dynamics of
11 Adsorbed CO₂ Species in Amine-Modified Porous Silica by Solid-State NMR Relaxation, J. Phys. Chem. C,
12 126, 12582–12591, <https://doi.org/10.1021/acs.jpcc.2c02656>, 2022.

13 Furman, G. B., Panich, A. M., and Goren, S. D.: Spin-locking in one pulse NMR experiment, Solid State
14 Nucl. Magn. Reson., 11, 225–230, [https://doi.org/10.1016/S0926-2040\(97\)00108-2](https://doi.org/10.1016/S0926-2040(97)00108-2), 1998.

15 Glaser, S. J., Boscain, U., Calarco, T., Koch, C. P., Köckenberger, W., Kosloff, R., Kuprov, I., Luy, B.,
16 Schirmer, S., Schulte-Herbrüggen, T., Sugny, D., and Wilhelm, F. K.: Training Schrödinger’s cat: quantum
17 optimal control, Eur. Phys. J. D, 69, 279, <https://doi.org/10.1140/epjd/e2015-60464-1>, 2015.

18 Goldman, M. and Tekely, P.: Effect of radial RF field on MAS spectra, Comptes Rendus Académie Sci. -
19 Ser. IIC - Chem., 4, 795–800, [https://doi.org/10.1016/S1387-1609\(01\)01310-X](https://doi.org/10.1016/S1387-1609(01)01310-X), 2001.

20 Grant, C. V., Wu, C. H., and Opella, S. J.: Probes for high field solid-state NMR of lossy biological samples,
21 J. Magn. Reson., 204, 180–188, <https://doi.org/10.1016/j.jmr.2010.03.011>, 2010.

22 Guenneugues, M., Berthault, P., and Desvaux, H.: A Method for Determining B₁ Field Inhomogeneity. Are
23 the Biases Assumed in Heteronuclear Relaxation Experiments Usually Underestimated?, J. Magn. Reson.,
24 136, 118–126, <https://doi.org/10.1006/jmre.1998.1590>, 1999.

25 Gupta, R., Hou, G., Polenova, T., and Vega, A. J.: RF Inhomogeneity and how it Control CPMAS, Solid
26 State Nucl. Magn. Reson., 72, 17–26, <https://doi.org/10.1016/j.ssnmr.2015.09.005>, 2015.

27 Haeberlen, U. and Waugh, J. S.: Coherent Averaging Effects in Magnetic Resonance, Phys. Rev., 175,
28 453–467, <https://doi.org/10.1103/PhysRev.175.453>, 1968.

29 Hahn, E. L.: Spin Echoes, Phys. Rev., 80, 580–594, <https://doi.org/10.1103/PhysRev.80.580>, 1950.

30 Hartmann, S. R. and Hahn, E. L.: Nuclear Double Resonance in the Rotating Frame, Phys. Rev., 128,
31 2042–2053, <https://doi.org/10.1103/PhysRev.128.2042>, 1962.

32 Hoult, D. I.: Solvent peak saturation with single phase and quadrature fourier transformation, J. Magn.
33 Reson. 1969, 21, 337–347, [https://doi.org/10.1016/0022-2364\(76\)90081-0](https://doi.org/10.1016/0022-2364(76)90081-0), 1976.

1 Hu, Y., Cheng, K., He, L., Zhang, X., Jiang, B., Jiang, L., Li, C., Wang, G., Yang, Y., and Liu, M.: NMR-Based
2 Methods for Protein Analysis, *Anal. Chem.*, 93, 1866–1879,
3 <https://doi.org/10.1021/acs.analchem.0c03830>, 2021.

4 Hürlimann, M. D. and Griffin, D. D.: Spin Dynamics of Carr–Purcell–Meiboom–Gill-like Sequences in
5 Grossly Inhomogeneous B_0 and B_1 Fields and Application to NMR Well Logging, *J. Magn. Reson.*, 143,
6 120–135, <https://doi.org/10.1006/jmre.1999.1967>, 2000.

7 Joseph, D. and Griesinger, C.: Optimal control pulses for the 1.2-GHz (28.2-T) NMR spectrometers, *Sci.*
8 *Adv.*, 9, eadj1133, <https://doi.org/10.1126/sciadv.adj1133>, 2023.

9 Keeler, E. G. and McDermott, A. E.: Rotating Frame Relaxation in Magic Angle Spinning Solid State NMR,
10 a Promising Tool for Characterizing Biopolymer Motion, *Chem. Rev.*, 122, 14940–14953,
11 <https://doi.org/10.1021/acs.chemrev.2c00442>, 2022.

12 Kelz, J. I., Kelly, J. E., and Martin, R. W.: 3D-printed dissolvable inserts for efficient and customizable
13 fabrication of NMR transceiver coils, *J. Magn. Reson.*, 305, 89–92,
14 <https://doi.org/10.1016/j.jmr.2019.06.008>, 2019.

15 Krahn, A., Priller, U., Emsley, L., and Engelke, F.: Resonator with reduced sample heating and increased
16 homogeneity for solid-state NMR, *J. Magn. Reson.*, 191, 78–92,
17 <https://doi.org/10.1016/j.jmr.2007.12.004>, 2008.

18 Krushelnitsky, A., Gauto, D., Rodriguez Camargo, D. C., Schanda, P., and Saalwächter, K.: Microsecond
19 motions probed by near-rotary-resonance R1 ρ 15N MAS NMR experiments: the model case of protein
20 overall-rocking in crystals, *J. Biomol. NMR*, 71, 53–67, <https://doi.org/10.1007/s10858-018-0191-4>,
21 2018.

22 Krushelnitsky, A., Hempel, G., Jurack, H., and Mendes Ferreira, T.: Rocking motion in solid proteins
23 studied by the 15 N proton-decoupled R 1 ρ relaxometry, *Phys. Chem. Chem. Phys.*, 25, 15885–15896,
24 <https://doi.org/10.1039/D3CP00444A>, 2023.

25 Kupče, Ě., Keifer, P. A., and Delepierre, M.: Adiabatic TOCSY MAS in Liquids, *J. Magn. Reson.*, 148, 115–
26 120, <https://doi.org/10.1006/jmre.2000.2224>, 2001.

27 Kurauskas, V., Izmailov, S. A., Rogacheva, O. N., Hessel, A., Ayala, I., Woodhouse, J., Shilova, A., Xue, Y.,
28 Yuwen, T., Coquelle, N., Colletier, J.-P., Skrynnikov, N. R., and Schanda, P.: Slow conformational
29 exchange and overall rocking motion in ubiquitin protein crystals, *Nat. Commun.*, 8, 145,
30 <https://doi.org/10.1038/s41467-017-00165-8>, 2017.

31 Kurbanov, R., Zinkevich, T., and Krushelnitsky, A.: The nuclear magnetic resonance relaxation data
32 analysis in solids: General $R\ 1/R\ 1\ \rho$ equations and the model-free approach, *J. Chem. Phys.*, 135,
33 184104, <https://doi.org/10.1063/1.3658383>, 2011.

34 Lee, Y. K., Kurur, N. D., Helmle, M., Johannessen, O. G., Nielsen, N. C., and Levitt, M. H.: Efficient dipolar
35 recoupling in the NMR of rotating solids. A sevenfold symmetric radiofrequency pulse sequence, *Chem.*
36 *Phys. Lett.*, 242, 304–309, [https://doi.org/10.1016/0009-2614\(95\)00741-L](https://doi.org/10.1016/0009-2614(95)00741-L), 1995.

1 Levitt, M. H., Oas, T. G., and Griffin, R. G.: Rotary Resonance Recoupling in Heteronuclear Spin Pair
2 Systems, *Isr. J. Chem.*, 28, 271–282, <https://doi.org/10.1002/ijch.198800039>, 1988.

3 Lewandowski, J. R., Sass, H. J., Grzesiek, S., Blackledge, M., and Emsley, L.: Site-Specific Measurement of
4 Slow Motions in Proteins, *J. Am. Chem. Soc.*, 133, 16762–16765, <https://doi.org/10.1021/ja206815h>,
5 2011.

6 Lips, O., Privalov, A. F., Dvinskikh, S. V., and Fujara, F.: Magnet Design with High B_0 Homogeneity for
7 Fast-Field-Cycling NMR Applications, *J. Magn. Reson.*, 149, 22–28,
8 <https://doi.org/10.1006/jmre.2000.2279>, 2001.

9 Lowe, I. J.: Free Induction Decays of Rotating Solids, *Phys. Rev. Lett.*, 2, 285–287,
10 <https://doi.org/10.1103/PhysRevLett.2.285>, 1959.

11 Ma, P., Haller, J. D., Zajakala, J., Macek, P., Sivertsen, A. C., Willbold, D., Boisbouvier, J., and Schanda, P.:
12 Probing Transient Conformational States of Proteins by Solid-State R1p Relaxation-Dispersion NMR
13 Spectroscopy, *Angew. Chem. Int. Ed.*, 53, 4312–4317, <https://doi.org/10.1002/anie.201311275>, 2014.

14 Malinowski, E. R. and Pierpaoli, A. R.: Asymmetric spinning sidebands from coaxial cells in NMR spectra,
15 *J. Magn. Reson.* 1969, 1, 509–515, [https://doi.org/10.1016/0022-2364\(69\)90087-0](https://doi.org/10.1016/0022-2364(69)90087-0), 1969.

16 Maricq, M. M.: Application of average Hamiltonian theory to the NMR of solids, *Phys. Rev. B*, 25, 6622–
17 6632, <https://doi.org/10.1103/PhysRevB.25.6622>, 1982.

18 Marion, D., Gauto, D. F., Ayala, I., Giandoreggio-Barranco, K., and Schanda, P.: Microsecond Protein
19 Dynamics from Combined Bloch-McConnell and Near-Rotary-Resonance R1 Relaxation-Dispersion MAS
20 NMR, *ChemPhysChem*, 20, 276–284, <https://doi.org/10.1002/cphc.201800935>, 2019.

21 Massi, F. and Peng, J. W.: Characterizing Protein Dynamics with NMR R1pRelaxation Experiments, in:
22 *Protein NMR: Methods and Protocols*, edited by: Ghose, R., Springer, New York, NY, 205–221,
23 https://doi.org/10.1007/978-1-4939-7386-6_10, 2018.

24 Mehring, M.: *Principles of High Resolution NMR in Solids*, 2nd ed., Springer-Verlag, Berlin Heidelberg,
25 <https://doi.org/10.1007/978-3-642-68756-3>, 1983.

26 Nimerovsky, E. and Goldbourt, A.: Insights into the spin dynamics of a large anisotropy spin subjected to
27 long-pulse irradiation under a modified REDOR experiment, *J. Magn. Reson.*, 225, 130–141,
28 <https://doi.org/10.1016/j.jmr.2012.09.015>, 2012.

29 Nimerovsky, E., Becker, S., and Andreas, L. B.: Windowed cross polarization at 55 kHz magic-angle
30 spinning, *J. Magn. Reson.*, 349, 107404, <https://doi.org/10.1016/j.jmr.2023.107404>, 2023.

31 Nishiyama, Y., Hou, G., Agarwal, V., Su, Y., and Ramamoorthy, A.: Ultrafast Magic Angle Spinning Solid-
32 State NMR Spectroscopy: Advances in Methodology and Applications, *Chem. Rev.*,
33 <https://doi.org/10.1021/acs.chemrev.2c00197>, 2022.

34 Oas, T. G., Griffin, R. G., and Levitt, M. H.: Rotary resonance recoupling of dipolar interactions in solid-
35 state nuclear magnetic resonance spectroscopy, *J. Chem. Phys.*, 89, 692–695,
36 <https://doi.org/10.1063/1.455191>, 1988.

- 1 Odedra, S. and Wimperis, S.: Imaging of the B_1 distribution and background signal in a MAS NMR
2 probehead using inhomogeneous B_0 and B_1 fields, J. Magn. Reson., 231, 95–99,
3 <https://doi.org/10.1016/j.jmr.2013.04.002>, 2013.
- 4 Olejniczak, E. T., Vega, S., and Griffin, R. G.: Multiple pulse NMR in rotating solids, J. Chem. Phys., 81,
5 4804–4817, <https://doi.org/10.1063/1.447506>, 1984.
- 6 Öster, C., Kosol, S., and Lewandowski, J. R.: Quantifying Microsecond Exchange in Large Protein
7 Complexes with Accelerated Relaxation Dispersion Experiments in the Solid State, Sci. Rep., 9, 11082,
8 <https://doi.org/10.1038/s41598-019-47507-8>, 2019.
- 9 Palmer, A. G. and Massi, F.: Characterization of the Dynamics of Biomacromolecules Using Rotating-
10 Frame Spin Relaxation NMR Spectroscopy, Chem. Rev., 106, 1700–1719,
11 <https://doi.org/10.1021/cr0404287>, 2006.
- 12 Palmer, A. G. I.: NMR Characterization of the Dynamics of Biomacromolecules, Chem. Rev., 104, 3623–
13 3640, <https://doi.org/10.1021/cr030413t>, 2004.
- 14 Palmer, A. G. I.: Enzyme Dynamics from NMR Spectroscopy, Acc. Chem. Res., 48, 457–465,
15 <https://doi.org/10.1021/ar500340a>, 2015.
- 16 Paulson, E. K., Martin, R. W., and Zilm, K. W.: Cross polarization, radio frequency field homogeneity, and
17 circuit balancing in high field solid state NMR probes, J. Magn. Reson., 171, 314–323,
18 <https://doi.org/10.1016/j.jmr.2004.09.009>, 2004.
- 19 Pratihaar, S., Sabo, T. M., Ban, D., Fenwick, R. B., Becker, S., Salvatella, X., Griesinger, C., and Lee, D.:
20 Kinetics of the Antibody Recognition Site in the Third IgG-Binding Domain of Protein G, Angew. Chem.
21 Int. Ed., 55, 9567–9570, <https://doi.org/10.1002/anie.201603501>, 2016.
- 22 Privalov, A. F., Dvinskikh, S. V., and Vieth, H.-M.: Coil Design for Large-Volume High- B_1 Homogeneity for
23 Solid-State NMR Applications, J. Magn. Reson. A, 123, 157–160,
24 <https://doi.org/10.1006/jmra.1996.0229>, 1996.
- 25 Quinn, C. M. and McDermott, A. E.: Monitoring conformational dynamics with solid-state $R_{1\rho}$
26 experiments, J. Biomol. NMR, 45, 5–8, <https://doi.org/10.1007/s10858-009-9346-7>, 2009.
- 27 Rangadurai, A., Szymaski, E. S., Kimsey, I. J., Shi, H., and Al-Hashimi, H. M.: Characterizing micro-to-
28 millisecond chemical exchange in nucleic acids using off-resonance $R_{1\rho}$ relaxation dispersion, Prog. Nucl.
29 Magn. Reson. Spectrosc., 112–113, 55–102, <https://doi.org/10.1016/j.pnmrs.2019.05.002>, 2019.
- 30 Redfield, A. G.: On the Theory of Relaxation Processes, IBM J. Res. Dev., 1, 19–31,
31 <https://doi.org/10.1147/rd.11.0019>, 1957.
- 32 Rovó, P.: Recent advances in solid-state relaxation dispersion techniques, Solid State Nucl. Magn.
33 Reson., 108, 101665, <https://doi.org/10.1016/j.ssnmr.2020.101665>, 2020.
- 34 Rovó, P. and Linser, R.: Microsecond Timescale Protein Dynamics: a Combined Solid-State NMR
35 Approach, ChemPhysChem, 19, 34–39, <https://doi.org/10.1002/cphc.201701238>, 2018.

- 1 Schanda, P. and Ernst, M.: Studying dynamics by magic-angle spinning solid-state NMR spectroscopy:
2 Principles and applications to biomolecules, *Prog. Nucl. Magn. Reson. Spectrosc.*, 96, 1–46,
3 <https://doi.org/10.1016/j.pnmrs.2016.02.001>, 2016.
- 4 Schmidt-Rohr, K., Clauss, J., and Spiess, H. W.: Correlation of structure, mobility, and morphological
5 information in heterogeneous polymer materials by two-dimensional wideline-separation NMR
6 spectroscopy, *Macromolecules*, 25, 3273–3277, <https://doi.org/10.1021/ma00038a037>, 1992.
- 7 Schönzart, J., Han, R., Gennett, T., Rienstra, C. M., and Stringer, J. A.: Magnetic Susceptibility Modeling of
8 Magic-Angle Spinning Modules for Part Per Billion Scale Field Homogeneity, *J. Magn. Reson.*, 364,
9 107704, <https://doi.org/10.1016/j.jmr.2024.107704>, 2024.
- 10 Sekhar, A. and Kay, L. E.: An NMR View of Protein Dynamics in Health and Disease, *Annu. Rev. Biophys.*,
11 48, 297–319, <https://doi.org/10.1146/annurev-biophys-052118-115647>, 2019.
- 12 Shaka, A. J., Keeler, J., Frenkiel, T., and Freeman, R.: An improved sequence for broadband decoupling:
13 WALTZ-16, *J. Magn. Reson.* 1969, 52, 335–338, [https://doi.org/10.1016/0022-2364\(83\)90207-X](https://doi.org/10.1016/0022-2364(83)90207-X), 1983.
- 14 Shcherbakov, A. A., Brousseau, M., Henzler-Wildman, K. A., and Hong, M.: Microsecond Motion of the
15 Bacterial Transporter EmrE in Lipid Bilayers, *J. Am. Chem. Soc.*, 145, 10104–10115,
16 <https://doi.org/10.1021/jacs.3c00340>, 2023.
- 17 Sodickson, A. and Cory, D. G.: Shimming a High-Resolution MAS Probe, *J. Magn. Reson.*, 128, 87–91,
18 <https://doi.org/10.1006/jmre.1997.1218>, 1997.
- 19 Stief, T., Vormann, K., and Lakomek, N.-A.: Sensitivity-enhanced NMR ¹⁵N R1 and R1ρ relaxation
20 experiments for the investigation of intrinsically disordered proteins at high magnetic fields, *Methods*,
21 223, 1–15, <https://doi.org/10.1016/j.ymeth.2024.01.008>, 2024.
- 22 Stringer, J. A., Bronnimann, C. E., Mullen, C. G., Zhou, D. H., Stellfox, S. A., Li, Y., Williams, E. H., and
23 Rienstra, C. M.: Reduction of RF-induced sample heating with a scroll coil resonator structure for solid-
24 state NMR probes, *J. Magn. Reson.*, 173, 40–48, <https://doi.org/10.1016/j.jmr.2004.11.015>, 2005.
- 25 Tekely, P. and Goldman, M.: Radial-Field Sidebands in MAS, *J. Magn. Reson.*, 148, 135–141,
26 <https://doi.org/10.1006/jmre.2000.2215>, 2001.
- 27 Tošner, Z., Porea, A., Struppe, J. O., Wegner, S., Engelke, F., Glaser, S. J., and Reif, B.: Radiofrequency
28 fields in MAS solid state NMR probes, *J. Magn. Reson.*, 284, 20–32,
29 <https://doi.org/10.1016/j.jmr.2017.09.002>, 2017.
- 30 Tošner, Z., Sarkar, R., Becker-Baldus, J., Glaubitz, C., Wegner, S., Engelke, F., Glaser, S. J., and Reif, B.:
31 Overcoming Volume Selectivity of Dipolar Recoupling in Biological Solid-State NMR Spectroscopy,
32 *Angew. Chem. Int. Ed.*, 57, 14514–14518, <https://doi.org/10.1002/anie.201805002>, 2018.
- 33 Uribe, J. L., Jimenez, M. D., Kelz, J. I., Liang, J., and Martin, R. W.: Automated test apparatus for bench-
34 testing the magnetic field homogeneity of NMR transceiver coils, *J. Magn. Reson. Open*, 18, 100142,
35 <https://doi.org/10.1016/j.jmro.2023.100142>, 2024.

- 1 Vera, Marisol. and Grutzner, J. B.: The Taylor vortex: the measurement of viscosity in NMR samples, J.
2 Am. Chem. Soc., 108, 1304–1306, <https://doi.org/10.1021/ja00266a035>, 1986.
- 3 Vold, R. L., Waugh, J. S., Klein, M. P., and Phelps, D. E.: Measurement of Spin Relaxation in Complex
4 Systems, J. Chem. Phys., 48, 3831–3832, <https://doi.org/10.1063/1.1669699>, 1968.
- 5 Vugmeyster, L., Ostrovsky, D., Greenwood, A., and Fu, R.: Deuteron rotating frame relaxation for the
6 detection of slow motions in rotating solids, J. Magn. Reson., 337, 107171,
7 <https://doi.org/10.1016/j.jmr.2022.107171>, 2022.
- 8 Vugmeyster, L., Rodgers, A., Ostrovsky, D., James McKnight, C., and Fu, R.: Deuteron off-resonance
9 rotating frame relaxation for the characterization of slow motions in rotating and static solid-state
10 proteins, J. Magn. Reson., 352, 107493, <https://doi.org/10.1016/j.jmr.2023.107493>, 2023.
- 11 Wang, A. C. and Bax, A.: Minimizing the effects of radio-frequency heating in multidimensional NMR
12 experiments, J. Biomol. NMR, 3, 715–720, <https://doi.org/10.1007/BF00198374>, 1993.
- 13 Xu, K., Pecher, O., Braun, M., and Schmedt auf der G nne, J.: Stable magic angle spinning with Low-Cost
14 3D-Printed parts, J. Magn. Reson., 333, 107096, <https://doi.org/10.1016/j.jmr.2021.107096>, 2021.
- 15 Zektzer, A. S., Swanson, M. G., Jarso, S., Nelson, S. J., Vigneron, D. B., and Kurhanewicz, J.: Improved
16 signal to noise in high-resolution magic angle spinning total correlation spectroscopy studies of prostate
17 tissues using rotor-synchronized adiabatic pulses, Magn. Reson. Med., 53, 41–48,
18 <https://doi.org/10.1002/mrm.20335>, 2005.